SHERGOTTITE PARENTAL MAGMA DEGASSING: INVESTIGATION OF LI ISOTOPES AND ABUNDANCES IN PYROXENE AND OLIVINE A. Udry[1] and H. Y. McSween Jr.[1], [1]Planetary Geosciences Institute, Dept. of Earth and Planetary Sciences, University of Tennessee, Knoxville, TN 37996, USA.

Introduction: Water degassing from shergottite parental magma can be investigated using lithium abundances and Li isotopes as shown by previous studies [e.g., 1-7]. Lithium is soluble in water-rich fluids and incompatible in pyroxene, olivine, and plagioclase during fractionation in dry systems [8]. Consequently, Li abundance profiles in shergottite pyroxenes will vary depending on whether the magma is dry or hydrated

Pyroxenes in shergottites underwent two-stages of crystallization: the cores crystallized at depth, separated by a halt in nucleation during magma ascent, and followed by formation of Fe-rich rims during or after eruption. During igneous fractionation in dry conditions, Li abundances in pyroxene rims will increase compared to pyroxene cores due to the fact that Li is incompatible in pyroxene. The multiple-stage pyroxene growth was thought to have been accompanied by magma water degassing [1,2,9]. Thus, if shergottite pyroxene crystallized from degassed previously water-rich magma, Li abundances will decrease from the core to the rim of the pyroxenes because lithium escapes with water.

Li isotopes (e.g., $^{7}Li/^{6}Li$, expressed relative to the L-SVEC standard as $\delta^{7}Li$) will be fractionated during magma degassing [3], ^{6}Li going preferentially into the gas phase compared to ^{7}Li. Therefore, degassing from a water-rich shergottite parental magma will be reflected as an increase of $\delta^{7}Li$ from pyroxene cores to the rims.

In order to investigate magma degassing in shergottite parental magmas, we are using geochemically distinct shergottites, which have various crystallization ages, magma source regions (which can be enriched or depleted), major and trace element compositions, as well as mineral modes.

Samples used in this study: We analyzed four compositionally different shergottites that span the age range of shergottites.

- Shergotty is a 165 ± 4 Ma enriched basaltic shergottite. Similar to the other basaltic shergottites, it consists of pyroxene and maskelynite [10]. Previous studies show that its parent magma was water-rich prior to eruption [9]

- QUE (Queen Alexandra Range) 94201 is a 327 ± 10 Ma depleted basaltic shergottite representing a liquid composition. [11]. Similarly to Shergotty, it exhibited a high water content before degassing [9].

- LAR 06319 is a 193 ± 20 Ma enriched olivine-phyric shergottite [12]. It consists of olivine megacrysts, groundmass pyroxenes and olivines, and maskelynite. Similar to QUE 94201, it represents a composition that underwent very limited crystal accumulation [13].

- Tissint is a depleted olivine-phyric shergottite and was recently dated at 574 ± 20 Ma representing the oldest shergottite [14].

Methods: Major compositions were analyzed using the CAMECA SX-100 electron microprobe at the University of Tennessee. Mineral compositions were determined using an accelerating voltage of 15 kV; beam current of 20 nA; counting times of 20 s except for Ca (30 s), Cr (30 s) and Ni (40 s) in olivine, and beam sizes of 1-2 µm (pyroxene and olivine), using standard PAP corrections.

Li abundances and isotopes were measured on a Cameca IMS-6f ion microprobe at Arizona State University (ASU). Ion microprobe analyses were conducted with a 10 nA O-beam with a spot diameter of 50 to 60 µm. Areas of interest were pre-sputtered for ~4 minutes to achieve steady-state count rates. Trace ion intensities (normalized to the $^{30}Si^{+}$ count rate) were used to determine concentrations. The counts at the masses of interest, i.e., $^{7}Li^{+}$ and $^{30}Si^{+}$, were integrated for 2 for each cycle and each measurement consisted of 20 cycles. Each isotopic analysis consisted of 100 cycles of measurement for ^{6}Li and ^{7}Li.

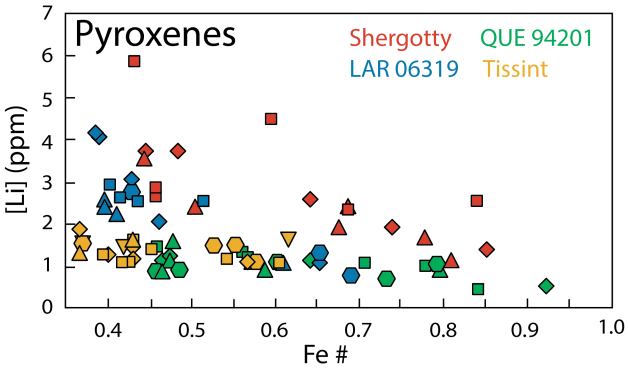

Fig. 1. Lithium abundances vs. Fe# in Shergotty, QUE 94201, LAR 06319, and Tissint pyroxenes. Each symbol represents a single pyroxene. Lithium abundances in pyroxenes decrease with increasing Fe# .

Results and Discussion:

Li abundances. For the four shergottites, Li abundances generally decrease from cores to the rims of pyroxenes. Additionally, Li abundances are inversely proportional to the pyroxene Fe# (Fig. 1). These patterns are indicative of magma degassing.

In addition to pyroxenes, we measured Li abundances in LAR 06319 and Tissint olivine megacrysts. Olivines in both shergottites show an increase of Li from core to rim as well as a positive correlation of lithium with Fe# (Fig. 2). These lithium trends represent normal igneous fractionation and thus, it appears that olivines were not affected by degassing. This result is consistent with the fact that olivines in olivine-phyric shergottites are thought to have fully crystallized prior to magma ascent and so before potential magma degassing [15].

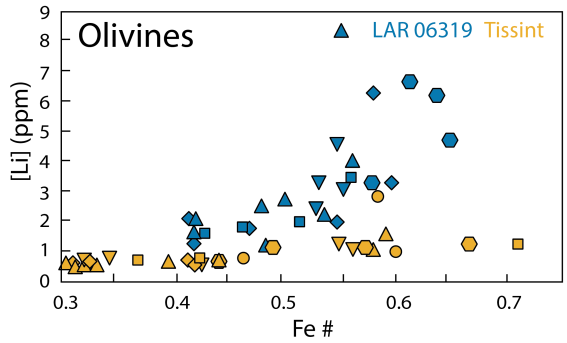

Fig. 2. Lithium abundances vs. Fe# in LAR 06319 and Tissint olivines. Each symbol represents a single olivine. Lithium abundances increase with Fe#.

Li isotopes. For the four shergottites, most of pyroxenes show an increase of δ^7Li from core to rims. However, it is not a consistent pattern. For example, Shergotty pyroxenes show patterns that might indicate lithium sub-solidus diffusion. Lithium is a very mobile element with ^{6}Li diffusing faster than ^{7}Li [16]. In addition, δ^7Li does not correlate with [Li]. Thus, δ^7Li shows a more complicated story that involves more than simple degassing.

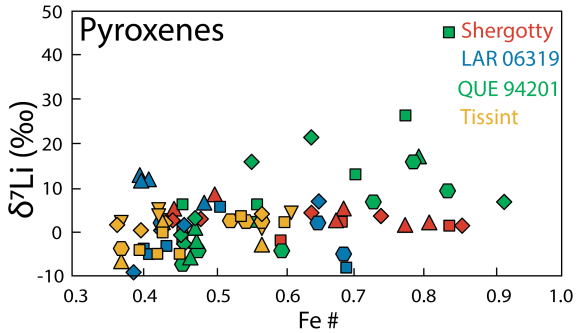

Fig. 3. δ^7Li (‰) vs. Fe# in Shergotty, QUE 94201, LAR 06319, and Tissint pyroxenes. Each symbol represents a single pyroxene. No clear correlation between δ^7Li and #Fe is observed.

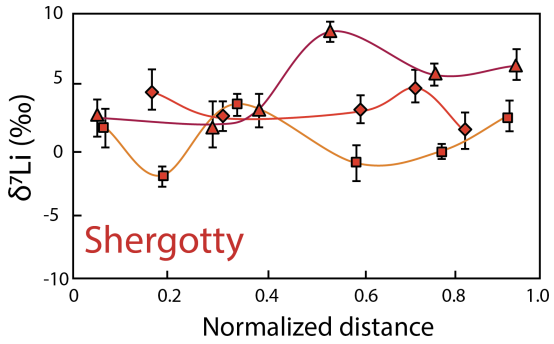

Fig. 4. δ^7Li (‰) vs. normalized in Shergotty pyroxenes. Each symbol represents a single pyroxene. Error bars are 2σ.

Acknowledgements: We thank Rick Hervig and Lynda Williams for their help with the SIMS analyses and Larry Taylor for providing the Tissint thin section.

References: [1] Lentz et al. (2001) *GCA*, 65, 4551-4565. [2] McSween et al. (2001) *Nature*, 409, 487-490. [3] Beck et al. (2004) *GCA*, 70, 2925-2933 [4] Herd et al. (2005) *GCA*, 69, 2431-2440. [5] Treiman et al. (2006) *GCA*, 70, 2919-2934. [6] Williams et al. (2010) *LPS XLI* Abstract #2641. [7] Anand and Parkinson (2010) *LPS XLI,* Abstract #2362 [8] Brenan et al. (1998) *GCA,* 62, 2129–2141. [9] McCubbin et al. (2012) *Geology,* 40, 683-886. [10] Stolper and McSween (1979) *GCA,* 43, 1475-1498 [11] McSween et al. (1996) *GCA,* 22, 4563–4569. [12] Shafer et al. (2010) *GCA,* 74, 7307-7328. [13] Basu Sarbadhikari et al. (2009) *GCA*, 73, 2190-2214. [14] Brennecka et al. (2014) *MAPS* 49, 412-418. [15] Balta et al. (2013) *MAPS,* 48, 1359-1382. [16] Richter et al. (2014) *GCA,* 126, 352-270.